DEVELOPMENT OF A MODERN BASE ISOLATION SYSTEM USING THE CONCEPT OF METAMATERIALS FUNCTIONAL FOR LOW-FREQUENCY SEISMIC WAVES

Submitted By

MUHAMMAD NAUMAN MASOOM (G.L)	**(245628)**
QURAT UL AIN KARIM	**(241893)**
IRTAZA BADAR	**(248328)**
AHMER NASEER	**(244724)**

BACHELOR'S IN CIVIL ENGINEERING

Year 2018-2022

Project Advisor:

Dr. Rao Arsalan Khushnood

Project Co-advisor:

Dr. Muhammad Usman

NUST Institute of Civil Engineering

School of Civil and Environmental Engineering

National University of Sciences and Technology, Islamabad, Pakistan

CERTIFICATION

This is to certify that the thesis entitled

DEVELOPMENT OF A MODERN BASE ISOLATION SYSTEM USING THE CONCEPT OF METAMATERIALS FUNCTIONAL FOR LOW-FREQUENCY SEISMIC WAVES

Submitted by

MUHAMMAD NAUMAN MASOOM (G.L)	**(245628)**
QURAT UL AIN KARIM	**(241893)**
IRTAZA BADAR	**(248328)**
AHMER NASEER	**(244724)**

Has been accepted towards the requirements

For the undergraduate degree in

Civil Engineering

_____

Dr. Rao Arsalan Khushnood

HOD Research

NUST Institute of Civil Engineering (NICE)

National University of Sciences and Technology, Islamabad, Pakistan

DECLARATION

We hereby declare that the thesis entitled “Development of a Modern Base Isolation System using the Concept of Metamaterial Functional for Low-Frequency Seismic Wave,” submitted by us, is based on the study and work done solely by us. All references to work done by any other person, institution, or source have been duly cited. We further clarify that this thesis has not been published or submitted for publication anywhere else.

ACKNOWLEDGEMENTS

In the name of Allah, the most merciful, the most compassionate, all praises be to Allah, the lord of the worlds, and prayers and peace be upon Muhammad (S.A.W), his servant and messenger.

Completing this project was possible only because of the blessings of Allah Almighty and the collaboration of many people to whom we are sincerely grateful.

We would like to thank our parents for their love and support and all the people that supported us during this project.

We would also like to pay a debt of gratitude to our advisor, Dr. Rao Arsalan, for the profound encouragement, support, and valuable time he provided for this work. He motivated us during the whole project and encouraged us in what we were doing. He provided us with guidance for countless hours; without him, this thesis would not have been written.

We owe our gratitude to Dr. Fawad Najam (NICE, NUST) for reviewing our work during many stages of our project and guiding us throughout. We would like to thank Dr. Muhammad Rizwan (HOD Structural Engineering, MCE, Risalpur), Engr. Huzaifa Umar Farooq (Lab Engr. Structural Dynamics Lab, MCE, Risalpur) for helping us with the testing is MCE, Risalpur.

Abstract

Seismology has seen a penetration of metamaterials for a breakthrough in vibrational wave manipulation which was not possible with the standard technology. Metamaterials are artificially engineered materials, or artificially engineered arrangement of conventional materials, yielding unconventional properties that cannot be realized inherently through conventional materials. Popularly used base isolation techniques in seismic wave mitigation fall short at low-frequency regions of the spectrum and fail to encompass both, flexible and rigid structures. Using the concept of metamaterials, the phenomena of local resonance and the Bragg scattering can create a stop band region of frequencies that undergo vibrational filtration. This study proposes a two-dimensional periodic foundation system that covers a wide and an ultra-low frequency region in its bandgap, enveloping the principal frequencies of seismic waves (i.e., 0.30 Hz to 7.35 Hz calculated analytically). Conducting experimental testing on the scaled-down prototype of the proposed foundation affirmed the mathematical model and the computational testing conducted on ANSYS by showing an average of 50% attenuation in the frequency band gap (i.e., 2.54 Hz to 8.08 Hz for the scaled-down version). At the resonant frequency, the experimentation showed a 73% attenuation. This study is a pioneer for setting the baseline for periodic foundations with the capability of fully mitigating the entire spectrum of seismic vibrational effects on structures.

Table of Contents

Table of Figures

Chapter one

Introduction

1.1 General

Metamaterials are defined as artificially engineered composite materials with modified microstructures that induce customized properties which are not intrinsically present in them. Stemming from the field of electromagnetics, metamaterials have entered the sphere of acoustics and seismology. This study proposes a foundation which uses acoustic metamaterials (or seismic metamaterials) to filter and control seismic waves.

Acoustic metamaterials have structures designed in a way that use the concept of local resonance to filter seismic waves within a specific frequency bandgap (locally resonant metamaterials). This bandgap lies near the resonant frequency of the locally resonant structure, which are tuned to resonate out of phase in the stopband region.

The proposed foundation uses steel cylinders with silicone pads as local resonators that are tuned to induce a resonant frequency. They exhibit the negative mass density phenomena with a sub-wavelength structure in the range of the stopband frequencies.

The local resonance is coupled with the mass-in-mass phenomena to accentuate the dissipation of wave energy. The dual stiffness of the steel cylinder and the silicone allows the resonator to act like a classical elastic solid which can be simplified as a mass-spring system. Locally resonant metamaterials exhibit negative mass if treated as a classical elastic solid.

Bragg diffraction is used in theoretical physics to describe the scattering of waves on periodic structures with sub-wavelength distances. Bragg's scattering adds another layer of vibrational control with the orderly spaced inclusions that simulate these periodic structures that scatter the incoming seismic waves.

Developing on the concept of composite foundations that couple the properties of periodic foundation and the conventional base isolation system [1], a proposal has been put forward for the formation of a two-dimensional periodic foundation system (for seismic waves that introduce lateral vibrations in the structure, to which the structure is most vulnerable) that covers a wide, as well as ultra-low frequency region in its bandgap, therefore enveloping the principal frequencies of seismic waves (0.2 Hz to 10 Hz). Such system caters for masonry, as well as long and short period concrete and steel structures. In addition, it has the

capability to safeguard some vital structures, such as nuclear power plants, which cause catastrophes in case of seismic failure when conventional base isolation system fails [2,3].

1.2 Problem Statement

Throughout the history, earthquakes have been a symbol of destruction and a headache for structural engineers. To make them less damaging, researchers have tried to devise a system that could mitigate the effect of seismic vibrations(1a)[4–6] Many different systems and devices have been proposed but the struggle to find a sustainable and effective seismic vibration control system continues. Out of all the techniques that have been proposed for seismic mitigation, a few stand out.

One such system is the Tuned Mass Damper (TMD) which has varying efficacy with the change in the type of earthquake [7]. Another is the conventional base isolation system, with efficacy decreasing with the increase in the flexibility of the structure. We have yet to find a system which is effective for all kinds of structure and covers the major region of the earthquake wave spectrum. Due to the limitations of conventional materials and methods, the development of such a system has not been possible. To overcome this issue, this study makes use of metamaterials with engineered properties that can provide vibrational filtration or vibrational mitigation not possible with conventional base isolation systems.

1.3 Objectives

The main objective of this research is to create a vibrational control mechanism for structures to mitigate the effects of seismic waves. The low-frequency region of the seismic wave spectrum is the main target, as it not catered for by conventional vibrational mitigation systems.

The research creates improvements on the conventional base isolation system to reach the targeted frequencies. This is done so by creating a periodic foundation that integrates the concept of metamaterials to filter out a band gap of seismic frequencies. So, consequently, the research also studies a major topic of metamaterials, the effects of local resonance and Bragg scattering on the attenuation caused by the foundation.

Another goal is to create a system that is compatible with all kinds of structures, both steel and concrete, and rigid and flexible.

The milestones set to achieve the goals are to study the mathematical model and integrate the mass in mass system concept into deriving the frequency band gap range. Then, constructing a scaled-down version of the proposed periodic foundation on ANSYS and analyzing the model to verify the frequency band gap

obtained from the mathematical model. And lastly, fabricating a laboratory-level scaled-down version of the proposed foundation and testing it on the shake table to affirm that the foundation will work under vibrational frequencies band gap of the scaled-down version.

1.4 Organization of the Report

The thesis begins with Chapter 1 discussing the major concept of metamaterials anchoring the periodic foundation proposed in the study, the objectives of the study and the overview of the thesis. Chapter 2 builds upon the general outline of the thesis, giving a deeper insight into the literature review conducted to support the thesis. Moving to Chapter 3, the thesis explains the materials and methodology used in the research, detailing the mathematical, computational, and experimental model and testing. The results of all three sets of model testing are addressed in Chapter 4, and the reasonings behind the specific outcomes are also highlighted. Chapter 5 concludes the entire research and outlines the key points of the work.

Chapter Two

Literature Review

2.1 Previous studies on metamaterials

Considering the gaps and limitations in traditional techniques for seismic vibration mitigation, continuous research is being conducted to improve these systems. Some of the improvements brought about in the base isolation system include negative-stiffness devices or dampers and low-cost elastic isolators among others [8–19]. A breakthrough in this field can be seen with the amalgamation of a new technology of metamaterials, that addresses the limitations of conventional systems.

Emanating from the field of electromagnetism, metamaterials have made their way into civil engineering and seismology. Metamaterials are artificially engineered materials, or artificially engineered arrangement of conventional material, yielding unconventional properties that cannot be realized inherently through conventional materials. In civil engineering, elastic metamaterials are being employed, which are artificial composite materials engineered to yield negative modulus, negative mass density or anisotropic mass under dynamic conditions to manipulate elastic waves [20–27]. Liu *et al.* in his study found that elastic metamaterial with a locally resonant structure in sonic crystal can result in negative mass density at or near the resonant frequency, which can be used to filter the propagation of wave within the bandgap [28]. The formation of this bandgap can primarily be attributed to either Bragg's scattering, or local resonance [28–30].

Bragg scattering, based upon Bragg's law, states that transmitted and reflected waves interfere destructively when the path difference between the two is not a multiple of the wavelength of the propagating waves[31] . Bragg scattering is usually easy to achieve and yields wider bandgaps compared to local resonance [32,33]. However, to achieve a strong destructive effect, it is critical for the phase difference between the transmitted and the reflected wave to be a multiple of half wavelength. This criterion of strong destructive interference is hard to achieve as the path difference depends upon the angle of incident wave. Also, to realize a strong destructive interference for seismic waves which have very low frequency (<50 Hz), a large system that requires a very large area is to be developed. Minor destructive interference, on the other hand, is easy to achieve.

Local resonance is another phenomenon that aids in vibrational manipulation. It uses local units or masses to dissipate the energy of the propagating wave through resonance and out-of-phase movement, relative to the medium in which it is placed. Consequently, it produces a bandgap in the vicinity of the resonant

frequency of the local masses[28,34]. While this phenomenon creates a more spatially efficient periodic system for low-frequency vibration control relative to the Bragg's scattering-based system, it is considered more complex to be devised. The latter proves to be more suitable while dealing with waves of low frequency [35–40], but ideally, both the phenomena can be made to interact to conceive wider bandgaps [41–44].

2.2 Using metamaterials in periodic systems

Inspired by the filtering effect of periodic systems accommodating the concept of metamaterials, several experimentations have shown the capability of such systems in manipulating seismic waves [45–47]. These systems can be further categorized as periodic wave barriers [48–53] and periodic foundations [1,54–66]. Both categorized systems have shown to be effective in vibration mitigation, where wave barriers are placed around the structure primarily to intercept surface waves, whereas periodic foundation are placed under the structure, designed to target any kind of seismic wave. A limitation of wave barrier is the amount of space it requires, but it can be an effective solution when a region is to be protected rather than a structure. In that case, the region has multiple structures with multiple time period, so the effectiveness of the wave barrier does not remain the same for each structure in that region.

The periodic foundations, also termed as locally resonant periodic foundation, have proven to be a viable solution for vibration control of the structure. They have drawn interest of many researchers and encourage the effort to devise a system to yield an expedient solution with minimal complications. One of the most significant and negative features of periodic functions is its ability to amplify the structural response in frequencies before the bandgap starts. Furthermore, no locally resonant periodic foundation has successfully been proposed yet that can cover long period waves (below 1 Hz).

2.3 Conventional vibrational control mechanisms

Conventional base isolation system has proven to be effective by laterally decoupling the structure from the ground it rests upon [67–70]. This technique is widely acknowledged and has also been incorporated into seismic design codes [71,72]. It works by reducing the lateral stiffness of the structure, thus elongating its natural period to avoid resonance with the expected seismic waves [73–76].

Despite being customary, the base isolation system comes with its own limitations. The base isolation system's effectiveness decreases with the increase in the flexibility of the structure. These systems are only good for structures which have a fixed base time period of less than or equal to 1 sec, as these structures provide a margin for the shift of period to a range of 1.5 sec to 3.5 sec, which makes them more flexible. An already flexible system does not provide further margin for flexibility. Hence, according to this

guideline of period to be 1 sec or less, only structures with around 10 or less stories can be isolated while yielding optimum performance [4,77,78]. Another limitation of this system is its lack of applicability to structures on soft soil. This is related to the properties of underlying soil on which the frequency of ground motion is dependent. In hard and stiff soils, the ground motion is rich with high frequency content while for soft soils, the ground motion consists of low frequencies. Base isolation works on the principle of elongating the period of a structure, hence making it more prone to resonance when used upon soft soils [4,77,79].

Another conventional vibrational control mechanism involves employing the tuned mass damper. They are primarily designed for wind loading but have also shown to be effective for seismic loading[80–82]. As vibrations are induced in the structure, the TMDs on top of the structure move out of phase. As a result, energy is dissipated with resonant vibrations of the damper. However, their efficacy varies with the type of earthquake, being noticeably effective only for earthquakes with low to medium intensity, in which the response is mainly governed by the fundamental vibration mode of the structure they are installed in [7]. With varying time and loading conditions, structures usually face variation in stiffness especially when they undergo elastoplastic behavior, which results in detuning of the TMDs. Even when the TMDs are optimized for elastoplastic behavior, their performance decreases with increase in the structural response's hysteretic portion [83–86]. Moreover, it has also been reported that the effectiveness of TMDs decreases as the PGA value goes up [87]. For PGA values greater than 0.176, effectivity can be as low as 10% [88].

Chapter Three

Materials and methodology

3.1 Materials and Proposed foundation panel

Figure 1 exhibits the top view of the proposed foundation panel. The proposed foundation panel is produced using high-density concrete embedded with steel-silicone resonators. The cross-sectional dimensions compute to 550 cm x 30 cm and the panel has square geometry. The panel comprises of a matrix of 96 resonators, each constituting of two parts: a 180 mm wide solid steel cylinder with a depth of 200 mm and a low stiffness silicone rubber. The silicone rubber is used as a barrier between the concrete panel and the solid steel cylinder. Adopting a large number of resonators allows the foundation to be a dense matrix of spatially ordered resonators that accelerate wave filtration. The center-to-center spacing of each circular inclusion is 30 cm since it carries the resonator. The specific distance is adopted in order to aid the wave manipulation process by ensuring the spatially ordered resonators have a distance smaller than the wavelength of the transmitted waves in the matrix. The panel is edged with 4 circular female ports, with diameter measuring at 63.5 cm. The underside of the panel comprises of 4 cylindrical concrete male side that extrude out of the panel to fit the female port. The female-male ports provide horizontal connections between different layers of the foundation. The female side of the ports have silicone rubber pads on the outer side instilled such that a male port from the overlaying panel can be adjusted between the faces of these rubber pads, thereby establishing a connection between them in the horizontal direction.

Table 1 Materials used in proposed foundation and their key parameters

Material	*Key Parameter*	*Value*
High density concrete	Density	$\rho = 3600$ kg/m^3
Steel Cylinder	Density	$\rho = 7850$ kg/m^3
Silicone Rubber	Youngs Modulus	E = 350 KPa
PTFE	Coefficient of friction	$\mu = 0.04$

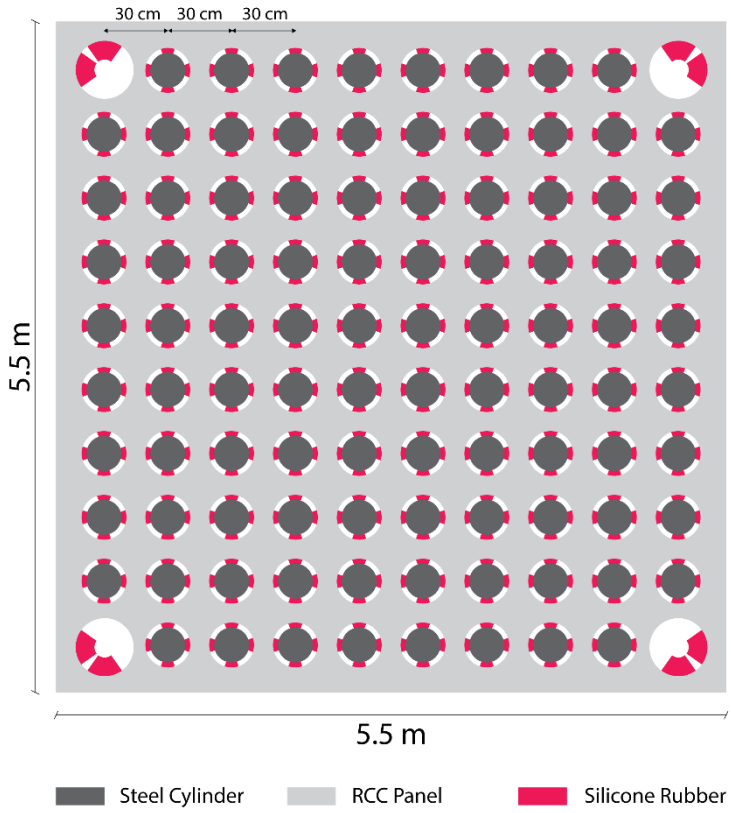

Figure 1. Top view of the proposed foundation panel containing a matrix of steel-silicone resonators

The panels are stacked on top of each other and are horizontally disconnected by frictionless, low-damping PTFE sheet on steel plates that cover the top and bottom of the panels. The stiffness in the horizontal direction is derived from the silicone rubber pads at the corner female ports. **Error! Reference source not found.** shows the materials used in the proposed foundation and their key parameters set to get the desired results.

3.2 Numerical Model

A simplified periodic mass-in-mass system represents the proposed foundation, with only one degree of freedom for each mass, while the whole system has multiple degrees of freedom. The simplified figure of this system is shown in Figure 2. The mass-in-mass system represents an internal mass within an external mass. The internal mass refers to the steel cylinders which are connected to the external mass, specifically the concrete in our panels, by internal springs that represent the silicone pads in the resonators. The external springs denote the silicone pads in the mechanical connections to assist in the horizontal

connection of the panels. Each mass-in-mass element denotes a singular concrete panel with resonators and connections embedded in it.

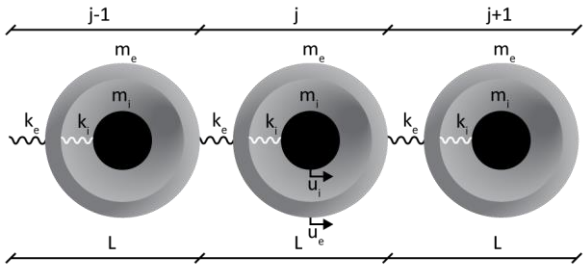

Figure 2. An idealized figure of the mass-in-mass system with the indication of m_i, m_e, k_i, and k_e. Where u_i and u_e represent the displacement of internal and external mass respectively. L represents the spatial period of the foundation in vertical direction.

This mass-in-mass idealized system can be solved based on the framework of variational approach (Energy approach), which uses the principle of virtual work in its dynamic form, also referred to as the Hamilton's principle to derive the Lagrange's equation of motion that can be applied in this case. It is given in equation 1.

$$\frac{\partial}{\partial t}\left(\frac{\partial T}{\partial \dot{u}_x}\right) - \frac{\partial T}{\partial u_x} + \frac{\partial U}{\partial u_x} = F_x \qquad (1)$$

Where T represents the kinetic energy, U represents the potential energy, and F represents the non-conservative force, which according to the given idealized system, will be taken equal to zero in our case as the system is conservative. $\dot{u}$ and u represent the velocity and displacement of the mass respectively.

The total kinetic energy for j-th element of periodic foundation is given as in equation 2.

$$T^j = \frac{1}{2} m \dot{u_r}^j + \frac{1}{2} m \dot{u_p}^j \qquad (2)$$

While the potential energy U is given by equation 3.

$$U^j = \frac{1}{2}k({u_r}^j - {u_p}^j)^2 + \frac{1}{2}k({u_p}^j - {u_p}^{j-1})^2 + \frac{1}{2}k({u_p}^{j+1} - {u_p}^j)^2 \quad (3)$$

Where subscript ‘r’ represents the internal resonator mass and subscript ‘p’ represents the external panel mass, Lagrange’s equation of motion for the j-th element can be written as in equation 4.

$$\begin{cases} \frac{\partial}{\partial t}\left(\frac{\partial T}{\partial \dot{u}_r{}^j}\right) - \frac{\partial T}{\partial {u_r}^j} + \frac{\partial U}{\partial {u_r}^j} = 0 \\ \frac{\partial}{\partial t}\left(\frac{\partial T}{\partial \dot{u}_p{}^j}\right) - \frac{\partial T}{\partial {u_p}^j} + \frac{\partial U}{\partial {u_p}^j} = 0 \end{cases} \quad (4)$$

The equations of motion are denoted in equation 5.

$$\begin{cases} m_r \ddot{u}_r{}^j + k_r\left({u_r}^j - {u_p}^j\right) = 0 \\ m_p \ddot{u}_p{}^j + k_r\left({u_p}^j - {u_r}^j\right) + k_p\left(2{u_p}^j - {u_p}^{j+1} - {u_p}^{j-1}\right) = 0 \end{cases} \quad (5)$$

According to Bloch’s theorem, for any structure that has infinite periodic units, the change in complex wave amplitude of a propagating wave without attenuation as it passes each unit cell, does not depend upon the location of the unit cell within the structure. Hence, the wave propagation through the entire lattice can be understood by considering only a single unit cell.[89] By considering the harmonic wave solution, the Lagrange equations of motion that have been derived can be further simplified by expressing the infinite periodic mass units in terms of a single j-th mass unit in the periodic chain using the concept of Bloch’s theorem. The generic solution for the equations of motion according to Bloch’s theorem are given as equation 6.

$$\begin{cases} u_r^{j+n} = B_r e^{i(qx+nqL-\omega t)} \\ u_p^{j+n} = B_p e^{i(qx+nqL-\omega t)} \end{cases} \quad (6)$$

where,

B_r and B_p are complex wave amplitude that account for any offset phase between the external and the internal masses.

q is the wave number

ω *is the angular frequency*

L is the spatial constant of periodic mass in mass system.

Considering Fourier space, the simplified equations in the matrix form are the ones shown in equation 7.

$$\begin{bmatrix} m_r & 0 \\ 0 & m_p \end{bmatrix} \begin{bmatrix} \ddot{B}_r^j \\ \ddot{B}_p^j \end{bmatrix} + \begin{bmatrix} -k_r & k_r \\ 2k_p(1-\cos qL) + k_r & -k_r \end{bmatrix} \begin{bmatrix} B_r^j \\ B_p^j \end{bmatrix} = 0 \quad (7)$$

The dispersion relationship of periodic mass in mass system is given in equation 8.

$$|k - m\omega^2| = 0$$

$$m_p m_r \omega^4 - \left[k_r\left(m_p + m_r\right) + 2k_p m_r(1-\cos qL)\right]\omega^2 + 2k_p k_r(1-\cos qL) = 0 \quad (8)$$

This dispersion relation gives the frequency region, in which the unit cells of the system can suppress the propagation of seismic waves, as the internal and external masses go out of phase. This region is said to be the frequency bandgap.[90,91] The start and the end frequencies of this region are given by the roots of the dispersion relation as shown in equation 9 and 10.

$$f_1 = \frac{1}{2\pi}\sqrt{\frac{[k_r(m_p + m_r)]}{m_p m_r}} \quad (9)$$

	$$f_2 = \frac{1}{2\pi}\sqrt{\frac{\left[k_r\left(m_p + m_r\right) + 4k_p m_r\right] - \sqrt{\left[k_r\left(m_p + m_r\right) + 4k_p m_r\right]^2 - 16 m_r m_p k_p k_r}}{2 m_p m_r}}$$	*10*

It is to be noted that qL is dimensionless wave number and is given in equation 11.

	$$qL = \alpha + i\beta$$	*11*

Here, the real part and the imaginary part are called the attenuation and the phase constants, respectively. The real part gives the rate of attenuation as the wave propagates from one unit cell to the other while phase constant gives the phase change through a unit cell. The displacement can be written in terms of attenuation and phase constants.

	$$u_x \propto e^{i(qx)}$$ $$u_x \propto e^{i((\alpha + i\beta)x/L)}$$ $$u_x \propto e^{i\alpha\,(x/L)} e^{-\beta\,(x/L)}$$	*12*

Hence, the displacement amplitude is directly proportional to $e^{-\beta\,(x/L)}$, which indicates the spatial decay of displacement exponentially with the factor β. Dimensionless wave number qL is also given in equation 13.

	$$qL = \cos^{-1}\left(1 - \frac{m_p m_r \omega^4 - \omega^2 k_r\left(m_p + m_r\right)}{2k_p m_r \omega^2 - 2k_p k_r}\right)$$	*13*

Thus, the theoretical attenuation can be given as the imaginary part of the dimensional wave number qL from equation 13.

3.3 Model Prototyping

The proposed periodic foundation panels could not be tested experimentally on the shake table due to the limitations in design specifications and the computational model required excessive computational power for assessment which was not possible to achieve. Hence, a scaled-down model prototype was prepared for computational as well as experimental validation, as shown in Figure 3. The scaled-down periodic foundation was experimentally and computationally tested, the purpose of which was to validate the dispersion relationship and not to predict the experimental results for the proposed foundation. Considering that, the scaling laws according to the principles of similitude (differential governing equation) can be relaxed to yield only partial similarity[92] since absolute similarity is mostly unachievable for real structures[93].

Table 2. Scale Factors for different parameters of the foundation

Scaled Property	*Expression*	*Scale Factor*
Mass of Panels	$\Lambda_{mp} = \frac{mp\ (scaled)}{mp\ (proposed)}$	$\frac{1}{85.17}$
Mass of Steel Resonator	$\Lambda_{mr} = \frac{mr\ (scaled)}{mr\ (proposed)}$	$\frac{1}{19}$
Combined Stiffness of Internal Rubber Pads	$\Lambda_{kr} = \frac{kr\ (scaled)}{kr\ (proposed)}$	$\frac{1}{19}$

Combined Stiffness of External Rubber Pads	$\Lambda_{kp} = \frac{kp\ (scaled)}{kp\ (proposed)}$	$\frac{1}{1}$

Modal parameters of internal resonators were kept constant while scaling down the proposed foundation panel. Using the scaling factors shown in Table, the length and width were scaled down to 1/5.5, while the depth of the panel to 2/3. The mass density of the panel was also decreased to 2/3. The bandgap of the scaled-down test model can be recalculated using the numerical model discussed above. k_p and k_r remain constant while m_r and m_p are scaled down.

Table 3 shows all the important similitude factors.

Table 3 Similitude Factors for scaled down foundation

Similitude Factor	*Ratio*
Length	1/5.5
Width	1/5.5
Depth	2/3
Area	1/30.25
Density	2/3
Mass of steel Resonator	5/96

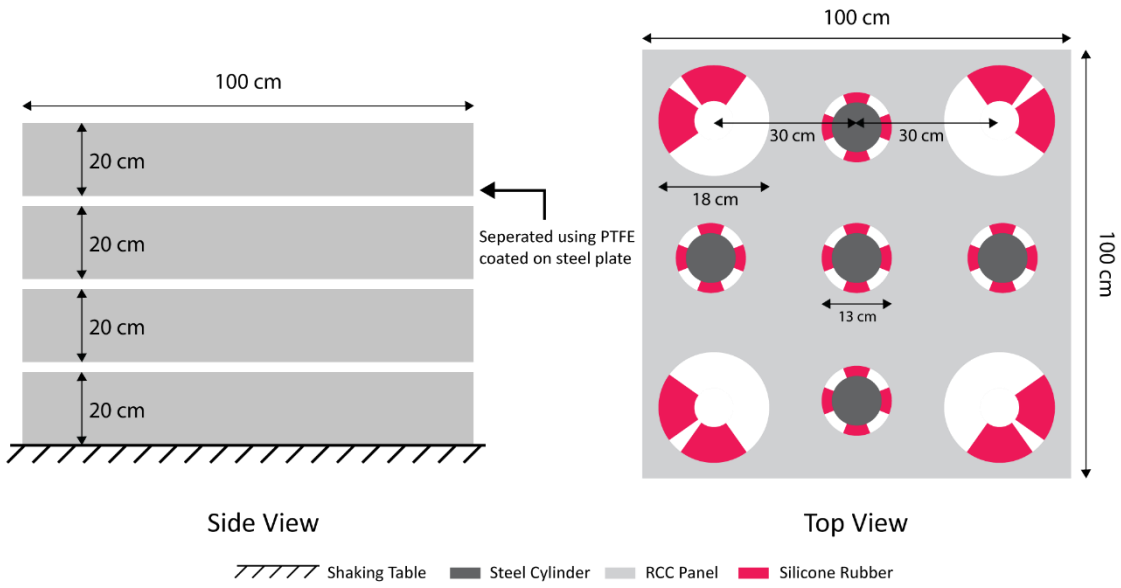

Figure 3. Side and top view of the scaled-down foundation having a total of three panels placed on the bottom panel, five steel-silicone resonators, and four corner connections.

Now, the scaled-down periodic foundation panel has a top surface area of 1 meter x 1 meter with a thickness of 20 cm, having 5 resonators with center-to-center spacing of 30 cm. The dimension and arrangement of the four male-female ports is the same as in the proposed foundation panel. The resonators were also of the same type and dimension as in the proposed foundation panel, with the steel cylinder in each resonator having a mass of approximately 21 kg.

The key properties of the scaled-down version of the proposed periodic foundation panel, on which the frequency bandgap according to the numerical model is dependent, are given in Table 4.

Table 4. Key parameters for the scaled down foundation

Property	*Expression*	*Value*
Mass of concrete panel	$m_p = \rho_c \times V_c$	$\rho_c = 2400$ kg/m^3 $V_c = 13.12 \times 10^{-2}\ m^3$ $m_p = 317\ kg$
Mass of steel cylinder	$m_r = n \times \rho_s \times V_s$	$\rho_s = 7850$ kg/m^3

		$V_s = 2.7 \times 10^{-3}\ m^3$ $n = 5$ $m_p = 106\ kg$
Stiffness of external silicone rubber pads	$k_p = 2 \times \frac{E_p \times A_p}{L_p}$	$E_p = 350 \times 10^3\ Pa$ $A_p = 3.75 \times 10^{-3}\ m^2$ $L_p = 8.75 \times 10^{-2}\ m$ $k_p = 3 \times 10^4\ \ N/m$
Stiffness of internal silicone rubber pads	$k_r = n \times \frac{E_r \times A_r}{L_r}$	$E_r = 350 \times 10^3\ Pa$ $n = 5$ $A_r = 3.00 \times 10^{-3}\ m^2$ $L_r = 2.5 \times 10^{-2}\ m$ $k_r = 210 \times 10^3\ \ N/m$

3.4 Computational Model

A computational model of the scaled-down periodic foundation was made to validate the analytical model as well as to check the feasibility of experimentation. The model was made using ANSYS software package. Harmonic analysis in the frequency domain was performed on the model to get the required information within the available computational power. The model geometry is shown in Figure 4. Key material properties required for the analysis were defined in the Table above (Model Similitude). All materials are linear and elastic. Contact nonlinearities are dealt by suitable contact elements.

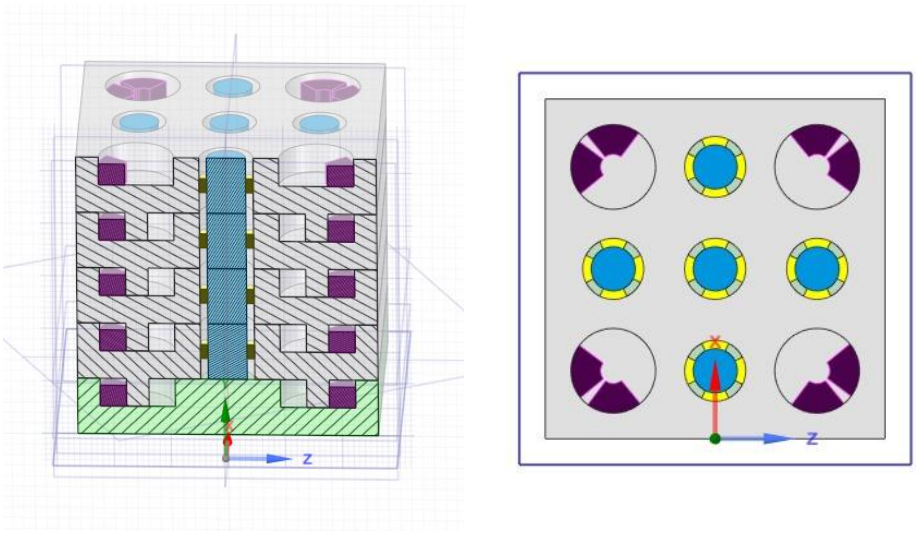

Figure 4. Computational model geometry of the scaled down foundation.

The frictionless behavior between the overlaying panels and steel cylinders inside the panels is simulated by introducing frictionless contact surfaces. The contact between the steel cylinder and the silicone rubber (in the resonator assembly), as well as between the cylindrical concrete male port and silicone pads of the female port was set to be frictional with a coefficient of friction equal to 0.6 to closely model the actual behavior, which allows normal movement away from the contact surface but resists normal movement towards the surface as well as tangential movement according to the set parameters. It was ensured that the softer surface with the finer mesh was chosen to be the contact surface. The behavior of the frictional contact was set to be symmetric to minimize the penetration, while other contact behaviors were set to asymmetric to reduce computational effort. Augmented Lagrange formulation was used to model contact behavior and stiffness. It is an iterative penalty method and results in constrained optimization.

Adaptive meshing was done to enhance computational efficiency, as shown in Figure 5. Mesh size was reduced to obtain a fine mesh at contact surfaces and silicone rubber pads, while a coarser mesh was used for target surfaces and parts where penetration was not an issue. The minimum orthogonal quality of mesh was 0.152, while the average orthogonal quality was 0.892, which is sufficient to yield accurate results. The maximum skewness was 0.73, which is acceptable. The total nodes formed were 338185, resulting in a total of 115489 triangular and quadrilateral elements.

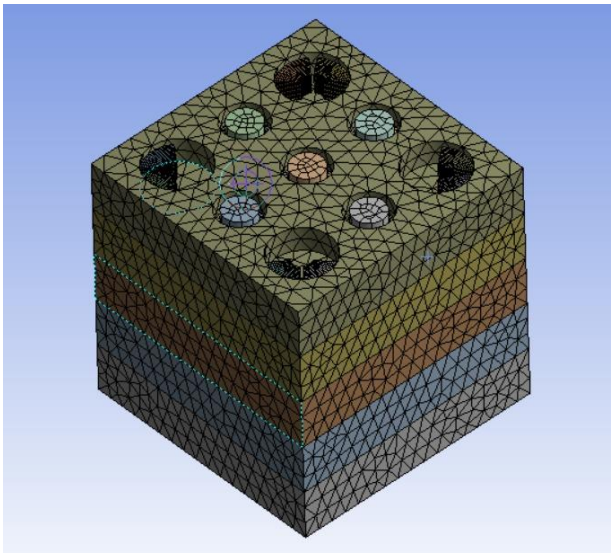

Figure 5. Visual depiction of meshing used in the computational analysis of scaled down foundation.

Mode superposition method was used for harmonic analysis to reduce computational power while ensuring efficiency. Max mode to be found was set to 100 between a frequency range from 0 to 12 Hz to get accurate results within the available resources. Analysis was done from 0 to 12 Hz with linear solution interval of 120.

The bottom of the base slab in the harmonic analysis was given a fixed boundary condition, while each steel cylinder was assigned roller support. A harmonic force was applied on the side face of the panel that was over the base slab, as it also replicates the force applied by the base slab through the connection port to the panel that lays over it. The force was kept as low as 12 KN to ensure no penetration resulting from high forces in contact surfaces while simulating the behavior of the periodic foundation, thus ensuring the accuracy of results. The frequency response curve was obtained and analyzed.

3.5 Experimentation

3.5.1 Experimentation Setup

For the experimental study, scaled-down periodic foundation was cast and assembled in the Structural Dynamics Lab MCE at NUST, Pakistan. The Shake table used for experimentation has a payload capacity of 12 tons and a maximum operating velocity of 1000 mm/sec.

The scaled-down periodic foundation for experimentation consists of a bottom panel (without resonators), which was fixed to the shaking table using 5 high strength bolts, and top panels with

resonators that were placed on the base slab and constrained in the horizontal direction using male-female port connections. The base panel also has female ports at the corner. The number of panels placed over the base panel was varied for the different testing arrangements, which will be discussed in the next section. Each panel was separated from its neighboring panel using an ultra-low damping frictionless surface realized with the help of a PTFE (Polytetrafluoroethylene) sheet that was fixed on steel plates connected to the top and bottom surfaces of the panel. PTFE allowed free movement of panels in the horizontal direction. Furthermore, grease was also applied to further ensure ultra-low damping surface. PTFE and grease were also used in the resonator assembly to ensure the internal masses were free to move independent of the panel, akin to the idealized analytical model.

The response of the tested foundation was recorded using a high-speed multi-channel data acquisition system and sensors consisting of accelerometers and displacement transducers (LVDTs). Triaxial wireless G-link-200 accelerometers were attached to each panel, shake table, and resonators of the top slab during the testing. The G-link-200 is a triaxial MEMS accelerometer with user-adjustable measurement range of **± 10g, ±20g, or ±40**. It has an extremely low noise density (80 µg/√Hz) and a resolution of 20 bits. It was used for continuous sample at rate of 128 Hz. Displacement of each panel and shake table was acquired using Micro-Measurements Model LDS-50 mm Linear Variable Differential Transformers (LVDTs). These LVDTs use strain gauge technology to record displacements by providing linearly proportional voltage based on the movements. LDS-50 mm has an accuracy of 0.2% with infinite resolution. The sampling rate for LVDTs was also set to 128 Hz. LVDTs were used to measure the relative displacement between the bottom panel and the other panels.

Figure 6 shows a detailed schematic of the testing setup used for each experiment.

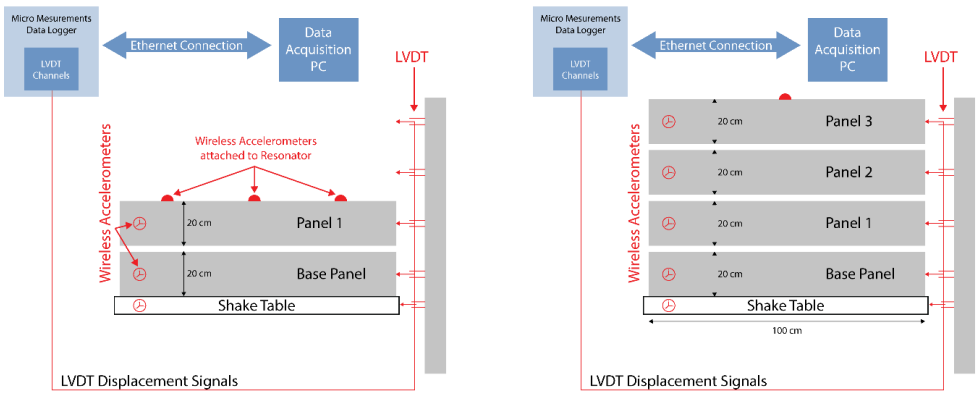

Setup for Experiment 1 & 2

Setup for Experiment 3

Figure 6. Simplified setup for the experiments showing all the equipment used during the testing.

Figure 7. Side view of the Casted Foundation

Figure 8. Top View of the Casted Foundation

3.5.2 Experimentation Procedure

The foundation was excited using simple harmonic motion. The maximum amplitude of sinusoidal displacement was set to 5 mm in order to capture the response with great accuracy, considering the available instrumentation. The response was recorded for frequencies between 0.5 to 9 Hz with an interval of 0.5 Hz.

In order to properly assess the harmonic response of the foundation and correctly draw the possible conclusions, the scaled-down periodic foundation was tested in three series of tests, as shown in Figure 9:

1. In the first series of tests, only one panel consisting of resonators was placed on the fixed base panel, and the assembly was excited using simple harmonic motion. The test had 2 objectives: to validate the analytical bandgap when only one panel was placed and to see the response in comparison to addition in the number of staked periodic foundation panels. (The test had 2 objectives, first to validate the analytical bandgap when only one panel was placed and second to see the response in comparison to when the number of periodic foundation panels with internal masses was increased). Accelerometers were placed on the shake table, panels as well as three out of 5 resonators to clearly understand their dynamics compared to the panel itself.

2. In the second series of tests, the previously tested panel was tested again; however, this time, the movements of the resonators were restricted using wooden pieces. These pieces were perfectly sized and shaped to block any movement of the resonators during the test. Such testing was done for the sake of comparison between a foundation panel in which the internal masses were free to

move and one in which the movement of the internal masses were restricted. However, later it was understood when the exceptional result yielded from this test were understood using the analytical model that by the introduction of wood, the system still behaves as a mass in mass system capable of producing a new bandgap with new starting and ending frequencies.

3. In the third series of tests, three panels placed on the fixed bottom slab were tested to compare the reduction in response as the number of the periodic foundation panels is increased. Again, one accelerometer was placed on one of the top panel resonators to record and assess its dynamics with respect to the panel it was contained in, while other available accelerometers were placed on all the 3 panels, base panel, and shake table.

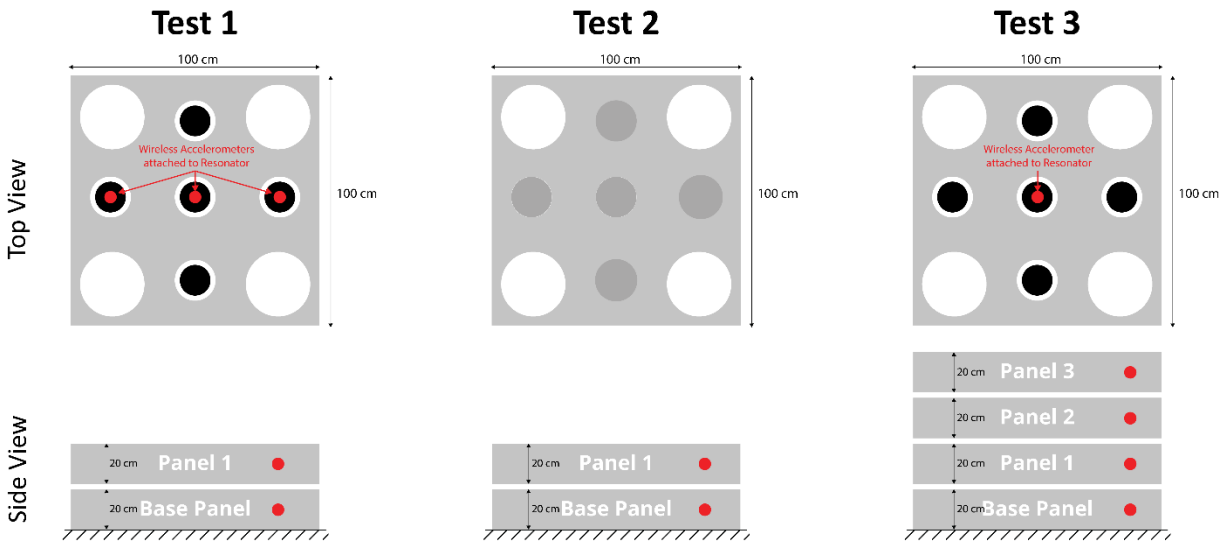

Figure 9. Schematic diagram showing placement of foundation panels and restraint conditions for resonators during each experiment.

Chapter Four

Results and discussions

4.1 Scaled Down Model

4.1.1 Theoritical Results

4.1.1.1 Scaled down periodic foundation (steel-silicone resonator)

As discussed earlier in section 2.3., for experimental and computational validation of the proposed periodic foundation panel, it was scaled down to a size that can be easily analyzed. According to the dispersion relationship obtained in section 2.2. the frequency bandgap that shall be attained by this scaled down version can be found using material constants as, $m_r = 106\ kg\ , m_p = 350\ kg, k_r = 210000\ \frac{N}{m}\ and\ k_p = 30000 \frac{N}{m}$.

The frequency bandgap starts at:

$$f_{start} = \frac{1}{2\pi}\sqrt{\frac{[k_r(m_p + m_r) + 4k_p m_r] - \sqrt{[k_r(m_p + m_r) + 4k_p m_r]^2 - 16 m_r m_p k_p k_r}}{2 m_p m_r}} = 2.54\ Hz \quad (14)$$

The frequency bandgap ends at:

$$f_{end} = \frac{1}{2\pi}\sqrt{\frac{[k_r(m_p + m_r)]}{m_p m_r}} = 8.08\ Hz \quad (15)$$

This frequency stop band is also illustrated in Figure 10 showing the dispersion curve computed from the dispersion relationship as the set of frequencies for increasing wave vector qL. The clear region between acoustical and optical branches clearly represents a bandgap from 2.54 to 8.08 Hz, which according to Bloch's theorem does not allow propagation of wave without being spatially attenuated across the infinite periodic unit cells.

Further, the Figure 11 shows the curve between attenuation factor β and frequency. The curve shows progressive increase in attenuation factor β with increase in the applied frequency within the bandgap region. β approaches its maximum at the natural frequency of the internal resonator, which is 7 Hz,

indicating that the maximum spatial attenuation of propagating wave as it travels through the periodic foundation will be achieved at the resonant frequency of internal mass. The attenuation factor is greater than zero for all frequencies in the bandgap region, hence theoretically strengthening the justification for achievement of the bandgap.

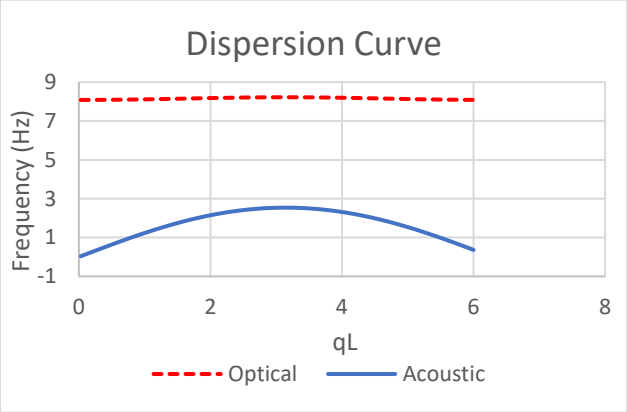

Figure 10. Dispersion Curve plotted between qL and Frequency for the resonator embedded scaled down periodic foundation

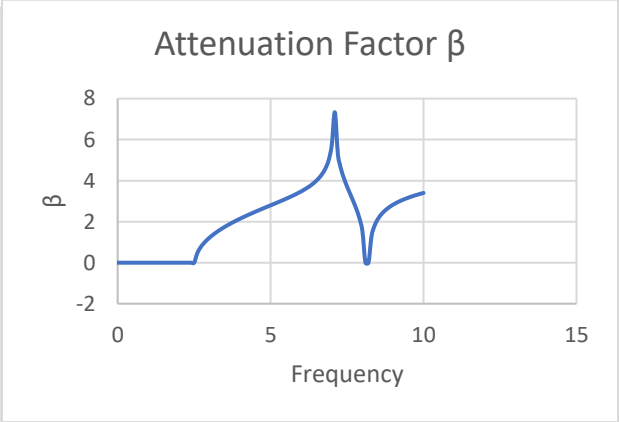

Figure 11. Graph between Frequency and Attenuation factor β for the resonator embedded scaled down periodic foundation

4.1.1.2 Scaled down periodic foundation (steel-wood arrangement)

In section 2.5.2. the restriction of the movement of steel cylinders using wooden pieces was discussed for the purpose of drawing comparison. It was later found out, as discussed in experimental results below, that by the introduction of wooden block a bandgap was attained. The analytical model was studied to find justification for this behavior, and it was realized that the dispersion relationship as derived in section 2.2. supports the experimental results when material properties for wood were included in the model. The following parameters were used in the model: $m_r = 106\ kg\ , m_p = 350\ kg, k_r = 7200000000\ \frac{N}{m}\ and\ k_p = 30000 \frac{N}{m}$. The theoretical bandgap for such foundation is shown in equation 12 and 13.

The frequency bandgap starts at:

$$f_{start} = \frac{1}{2\pi}\sqrt{\frac{[k_r(m_p + m_r) + 4k_p m_r] - \sqrt{[k_r(m_p + m_r) + 4k_p m_r]^2 - 16 m_r m_p k_p k_r}}{2 m_p m_r}} \quad (16)$$

$$= 2.58\ Hz$$

The frequency bandgap ends at:

	$$f_{end} = \frac{1}{2\pi}\sqrt{\frac{[k_r(m_p + m_r)]}{m_p m_r}} = 1497.2\ Hz$$	17

Hence, theoretically a very wide frequency stop band is obtained, and is a very useful finding. This system behaves as a mass in mass periodic structure. The dispersion curves driven through the dispersion relationship by varying the value of wave vector qL can be seen in the Figure 12. The ultra-wide region between the acoustical and optical branches illustrates the frequency stop band, in which according to Bloch's theorem, the wave propagation will result in spatial attenuation as it passes across the unit cell of the periodic chain.

The graph for attenuation factor β for increasing applied frequency on the periodic system is shown in the figure. Figure 13 shows that within the concerned frequency region of less than 10 Hz for seismic waves the attenuation factor has a value greater than zero, but when compared to attenuation factor in the figure when steel-silicone resonators were used, the value of attenuation coefficient β is equal for some frequencies and lesser for the rest, with a major difference near 7 Hz. No peak of attenuation factor β was attained in the concerned frequency band, because with wood instead of silicone, the natural frequency of the internal resonator becomes equal to 1311.7 Hz, hence the peak for attenuation factor β must be attained at this frequency.

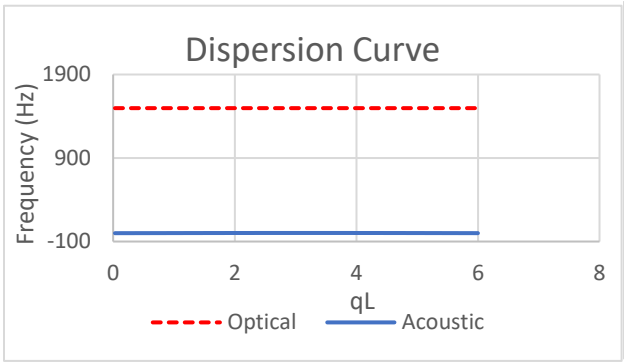

Figure 12. Dispersion Curve plotted between qL and Frequency for the restricted resonators scaled down periodic foundation

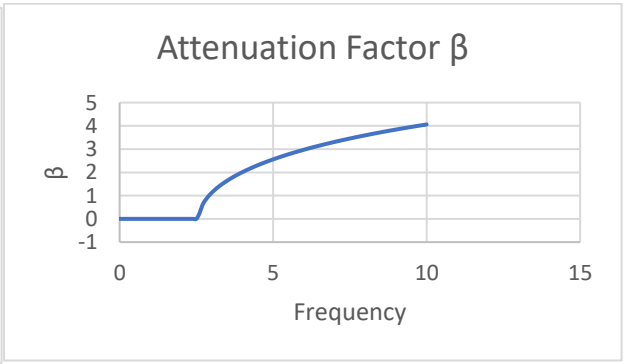

Figure 13. Graph between Frequency and Attenuation factor β for the restricted resonator scaled down periodic foundation

4.1.1.3 Effective mass of periodic foundation

A mass in mass unit as discussed previously can also be represented as a single unit. The term effective mass represents the mass of such a unit in a system that ignores the internal mass while integrating its effect in the effective mass. The expression for effective mass is given in equation 12.

	$$m_{eff} = m_p + \frac{m_r \omega_o}{{\omega_o}^2 - \omega^2}$$	*18*

Where, ω_o represents the resonant frequency of the internal resonator in $rads^{-1}$. A simplified single mass-spring system and its effective mass model is shown in Figure 14.Figure 14. Single spring-mass system and its effective mass model. It can be observed that as the applied frequency ω approaches the internal mass resonant frequency from below, the effective mass starts to increase in the bandgap region. The effective mass becomes unbound when applied frequency equals the internal mass resonant frequency and becomes negative as soon as the applied frequency approaches the internal mass resonant frequency from above. The increase and decrease of the effective mass can also be linked to the energy dissipation as when the effective mass becomes negative, the displacement negates the applied force in terms of direction.

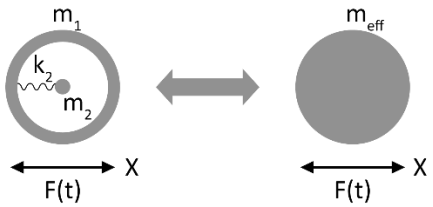

Figure 14. Single spring-mass system and its effective mass model.

The Figure 15 shows the comparison in the variation of effective mass of the scaled down periodic foundation. In the frequency region of interest, from 0 to 10 Hz, the foundation panel with steel-silicone resonators show great variation in effective mass within the bandgap region. Thus, the effective mass approaching infinity at the natural frequency of the resonator may result in greater energy dissipation as compared to the foundation panel with steel-wood resonator, whose effective mass has negligible variation in the concerned region due to very high resonant frequency of the internal mass.

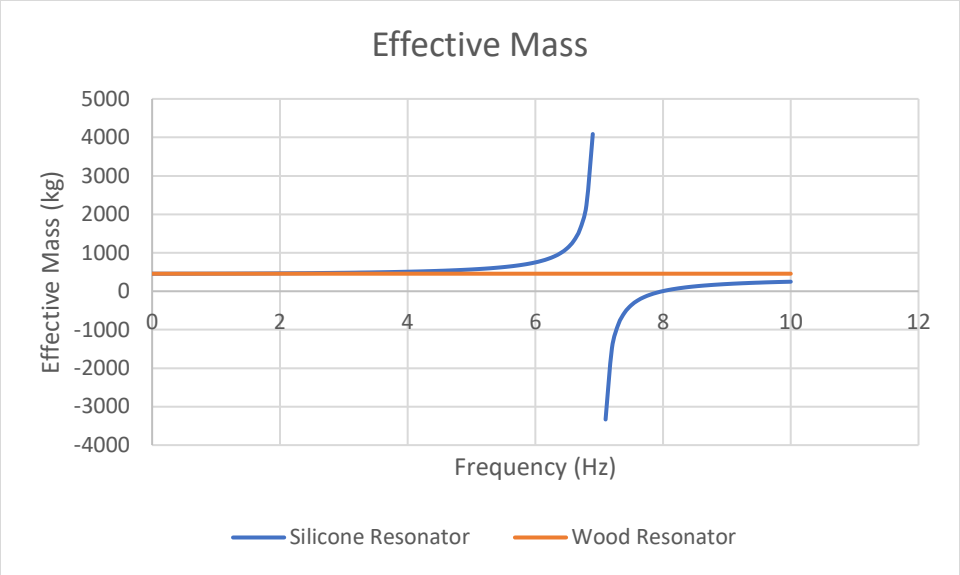

Figure 15. Comparison in the variation of effective mass of the scaled down periodic foundation.

4.1.2 Computational Results

A computational model was analyzed using ANSYS Mechanical to generate frequency response curve as discussed in section 2. 4.. The model was made with internal resonators as discussed previously. The Figure 16 shows the frequency response curve of the top and bottom foundation panel of both type of models. It is evident from the response curve that the modal frequencies of both top and bottom panels of the stacked foundation system with internal resonators have been shifted before the start of the bandgap and a bandgap is attained successfully (for bottom and top panels both) in the targeted region as claimed by the dispersion relationship in the analytical calculations. The periodic foundation shifts the oscillation periods as well as dissipates the energy of the waves passing through it with frequencies lying in the bandgap. The dissipation of energy is a result of the out of phase movement of the steel cylinders compared to the panel which contains them within the bandgap, local resonance at the resonant frequency of the internal mass and due to Bragg's scattering due to the symmetrical and periodic arrangement of the internal masses with spacing less than the wavelength it is subjected to. These computational results correspond with our analytical findings and support our claim of achieving a wide frequency band gap, covering the major portion of seismic wave frequency band.

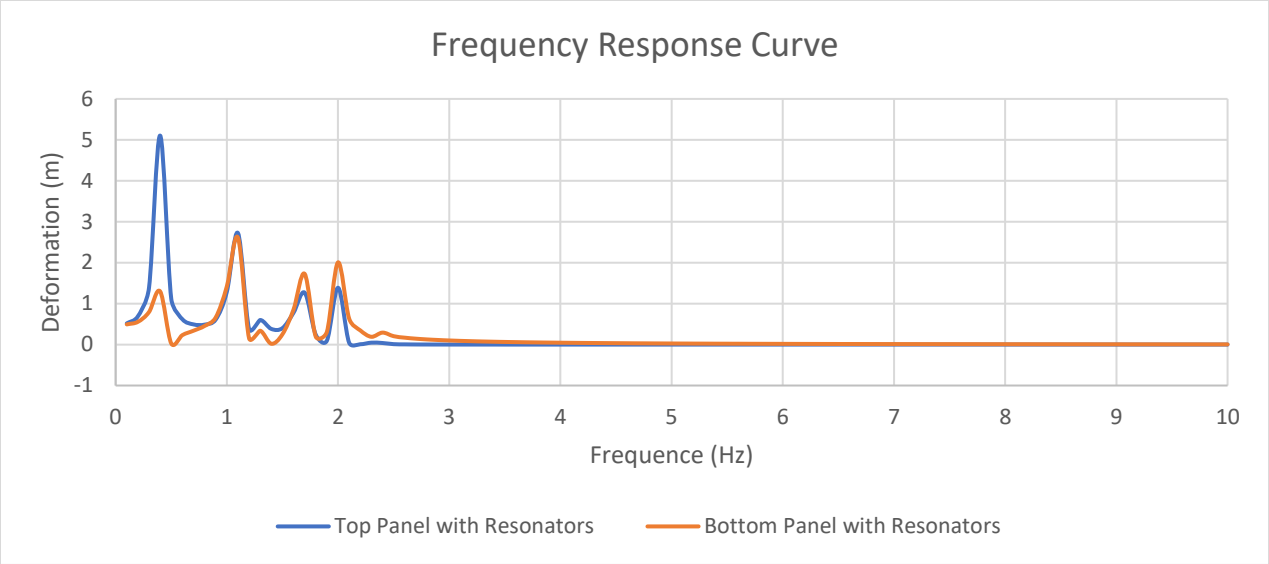

Figure 16. Frequency Response Curve for the top and bottom panel of the foundation embedded with resonators.

4.1.3 Experimental Results

As discussed in section 3.5.2 three series of testing were conducted for different arrangements of the periodic foundation panel. The key results have been summarized in Figure 17. Starting from the first two series of experimental testing in which only one periodic foundation panel was placed over the base slab that was fixed with the shake table. Test 1 had steel-silicone resonator while in Test 2 the movement of steel cylinders was restricted by wooden pieces. Figure 17 shows the comparison of displacement attenuation for both series of test. The attenuation was calculated as the percentage decrease in the maximum response of the top panel (which in both the cases was the first panel) compared to the displacement of base slab. For both the series of tests, the bandgap predicted analytically was achieved, with the first series of test generally showing greater attenuation in response (approximately 10% more at most of the frequencies) than the second series of test, except for 4 Hz where Test 2 tends to show slightly more attenuation than Test 1. The maximum attenuation of 62% was obtained for Test 1, while 50% for Test 2. Test 1 showed a greater attenuation since local resonance of the internal mass lies within the concerned frequency region. This justification is also backed by the attenuation factor β as discussed in section 4.1.2 and 4.1.3, where β shows generally greater attenuation within the bandgap region for steel-silicone resonator of Test 1. The attenuation can also be attributed to Bragg's scattering. Bragg's scattering occurs when wave passes through a space with periodic discontinuities or obstructions, with the distance between the discontinuities less than the wavelength of the passing wave, resulting in destructive interference of the reflected waves. The attenuation in both the series is a result of both, Bragg's scattering and local resonance. The maximum attenuation is still not achieved as the distance is not half

the wavelength. The question we ponder upon is why 10% of the attenuation is accorded to local resonance at the local resonant frequency, while the attenuation should have been greater according to attenuation factor β in section 4.1.2 and effective mass effect in section 4.1.4.

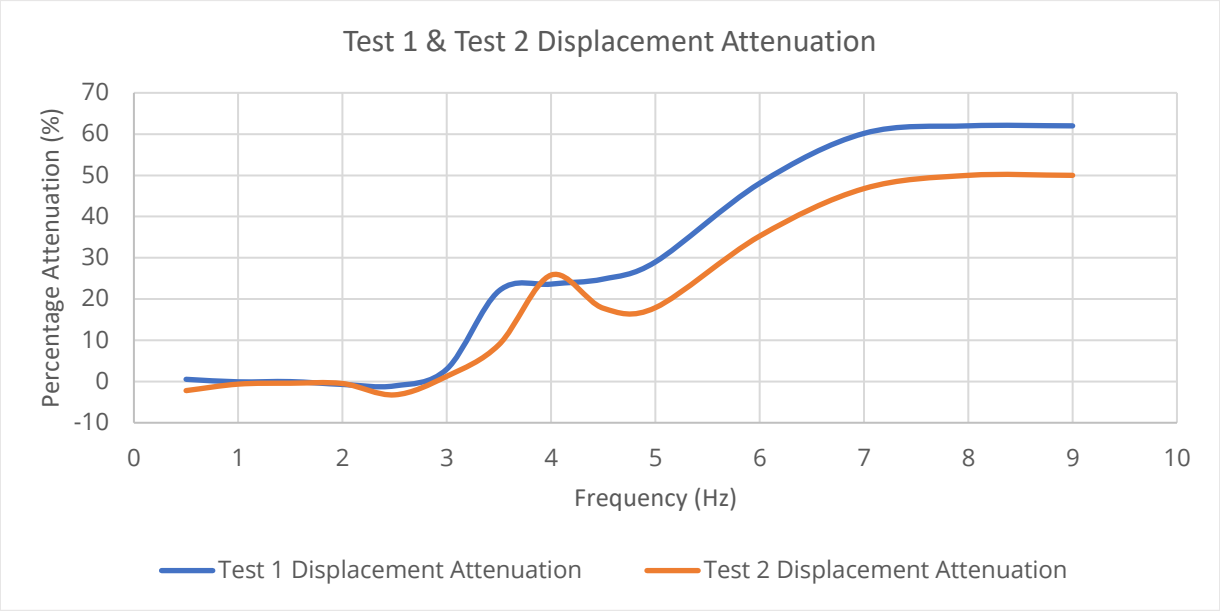

Figure 17. Comparison of Displacement Attenuation curve for Test 1 and Test 2

Figure 18 shows the time histories from the Test 1. One can visualize from Figure 18 a to c that with approximately negligible amplification at the start of bandgap, the displacement response tends to decrease as one goes much inside the bandgap. Figure 18 d is very important as it compares the time history of the top panel with the time history of the resonator that is in that panel at the resonant frequency of 7 Hz. The assumption was that when the foundation system is subjected to harmonic loading, the resonator must go in a harmonic motion, rather it goes into a periodic motion. As periodic motion is a sum of harmonic motion of different frequencies, it is now clear why attenuation only increases by 10% due to steel-silicone resonator. The periodic motion of the resonator in Figure 18 d is out-of-phase compared to the motion of the panel which contains it, resulting in energy dissipation. This energy dissipation must have been greater if the resonator had undergone a harmonic motion rather than a periodic motion.

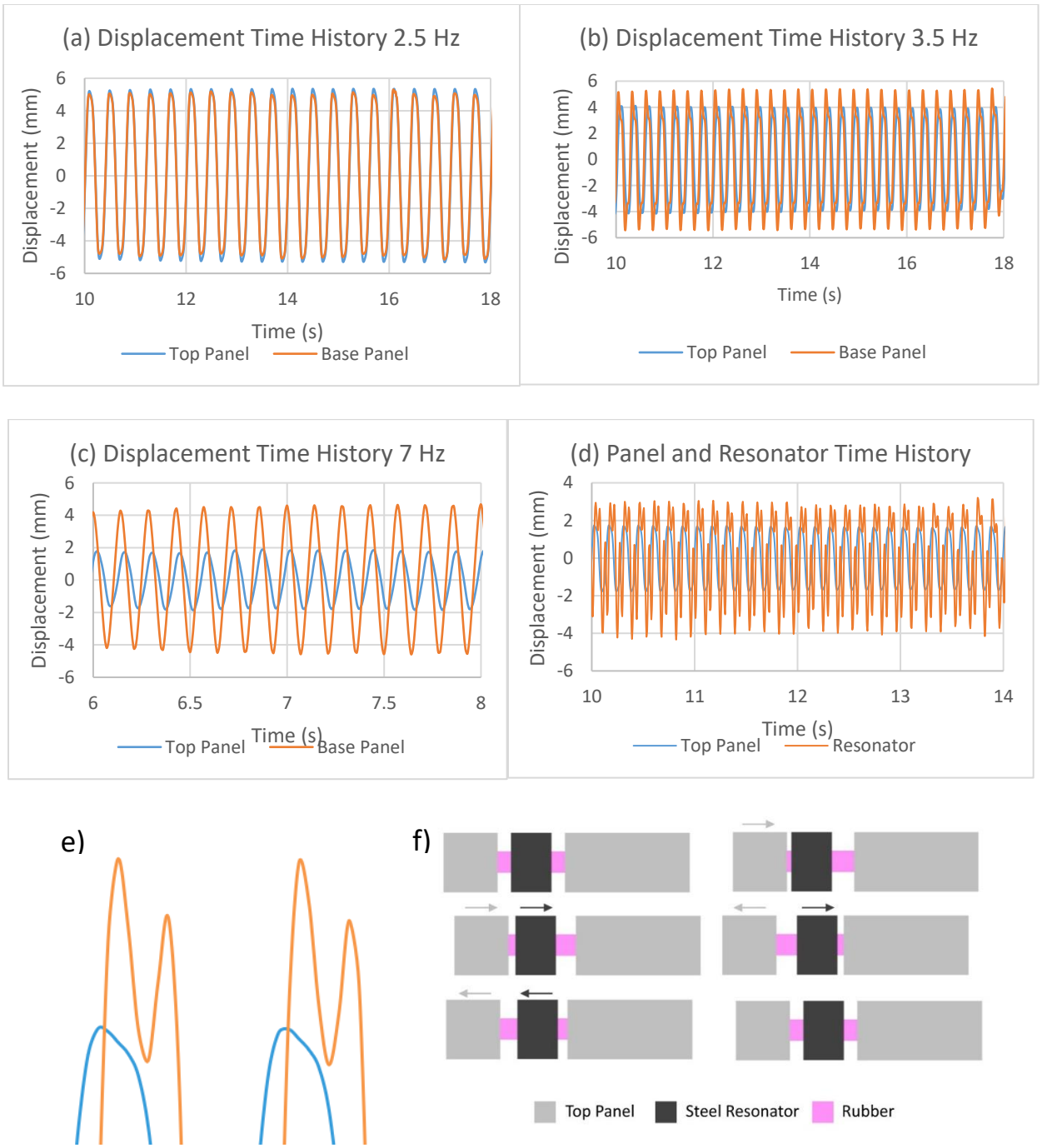

Figure 18.a) Displacement time history of top and base panel at 2.5 Hz. b) Displacement time history of top and base panel at 3.5 Hz. c) Displacement time history of top and base panel at 7 Hz. d) Time history comparison between top panel and resonator at 7 Hz. e) Extended view of the peak of time history comparison between top panel and resonator. f) Visual representation of the position of resonators with respect to the top panel during one cycle of movement.

Figure 19 shows the displacement attenuation curve from Test 3 in which three periodic foundation panels were stacked up on the base slab that was fixed to the shake table. An increase of an average 10%

can generally be observed in the attenuation observed at the top slab when compared to Test 1, which only had 1 panel. The maximum attenuation of 73% was observed near the resonant frequency of the internal mass. One may find it unusual that panel 1 has a higher attenuation than panel 3, with the highest attenuation for the bottom most panel. The most appropriate justification for this type of behavior is the load on top of these panels, which is significant (greater than 1000 kg on bottom panel, including the weight of steel plates). This normal load on the panel causes an increase in the frictional forces that are dependent on these normal forces, hence increasing the energy dissipation due to friction. About 20% increase in attenuation resulted in the bottom most panel just over the base slab when compared to Test 1, which only has one panel with no load over it.

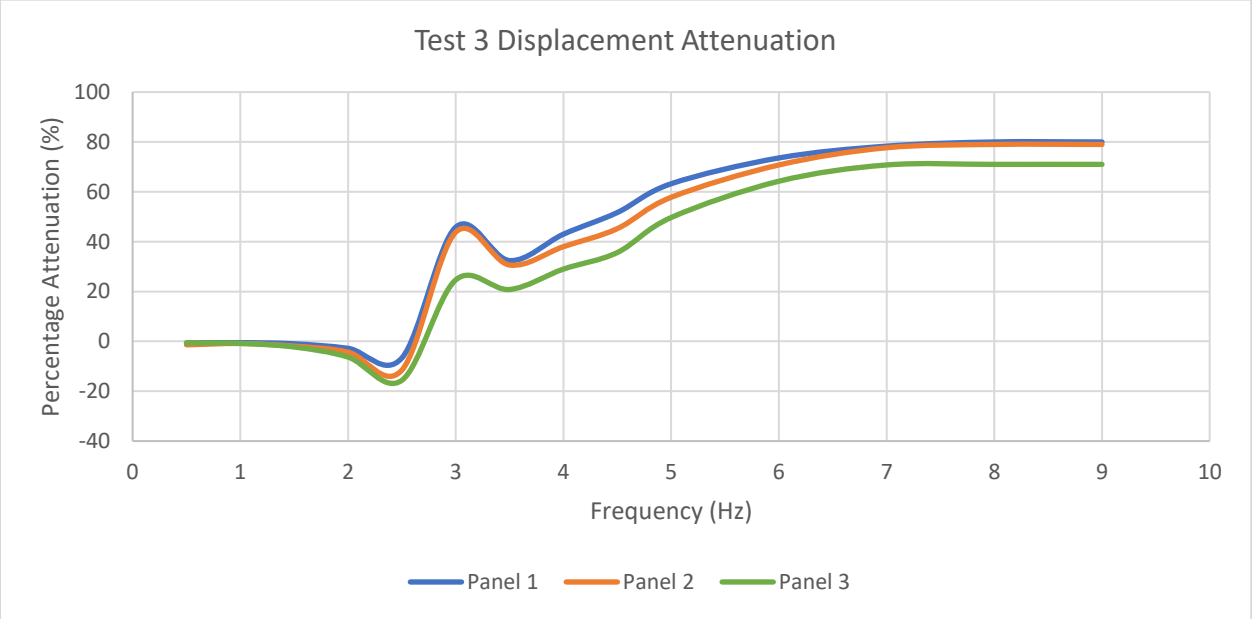

Figure 19. Displacement attenuation curve for each panel during Test 3.

The bandgap for the experimental foundation starts around 2.6 Hz and shows an average of 50% attenuation authenticating the enhancements made in the proposed foundation to be efficient with 3 panels. Casablanca's composite foundation CF with 4 layers produced a bandgap starting near 4.5 Hz and filtered more than 50% of the wave energy[1]. Sun's TID-equipped (tuned-inerter-damper TID) locally resonant periodic foundation LRPFs succeeded in achieving a reduction of average maximum response of 49% when tested for fuel storage tanks[94]. But the seismic performance of the foundation decreased by almost 20% when there is 20% deviation in the eigenfrequency as compared to the one the structure is designed for.

In 2021, Zhao achieved a maximum reduction of 49% of the peak horizontal acceleration response in a steel frame using periodic base isolation when tested experimentally and 35.6% when tested numerically.

The research concluded only a slight influence of the effect of increasing the unit cells, referring to two layers of rubber and concrete foundation, on the response of the structure due to lack of practically applicability on that level[95].

The proposed foundation in this paper, with improvements on the previous research has proven to be comparable or better at seismic mitigation.

The experimental results are the final strength that was required, which now enables us to draw the conclusion that based on scaled down testing it can be said that the proposed foundation would achieve the analytical bandgap. It was also observed that the start of frequency bandgap for system using very low stiffness rubber in lateral connection between different panel is majorly dependent on the stiffness of this mechanical connection rather the stiffness of the link connecting internal mass with the external mass (as seen in Test 2).

4.2 Proposed Foundation

4.2.1 Theoretical Results

4.2.1.1 Proposed Periodic Foundation (steel-silicone resonator)

The dispersion relationship obtained in section 2.2. can be used to find bandgap for the proposed and scaled down foundation both. Using $m_r = 2016\ kg\ , m_p = 30500\ kg, k_r = \ 4032000\frac{N}{m}\ and\ k_p = 30000\frac{N}{m}$ of the proposed periodic foundation, the bandgap illustrated in equation 12 and 13 was drawn.

The frequency bandgap starts at:

$$f_{start} = \frac{1}{2\pi}\sqrt{\frac{[k_r(m_p + m_r) + 4k_p m_r] - \sqrt{[k_r(m_p + m_r) + 4k_p m_r]^2 - 16 m_r m_p k_p k_r}}{2 m_p m_r}} = 0.30\ Hz \quad (19)$$

The frequency bandgap ends at:

$$f_{end} = \frac{1}{2\pi}\sqrt{\frac{[k_r(m_p + m_r)]}{m_p m_r}} = 7.35\ Hz \quad (20)$$

Figure 20 shows the dispersion curve for material constants of periodic foundation panel. There is a clear region between acoustical and optical mode representing the wide low frequency stop band that the proposed periodic foundation panel establishes, as obtained by the above equations as well. Figure 21 shows the curve between the attenuation factor β and frequency. Theoretically, the attenuation factor increases with the increase in applied wave frequency. It is of particular interest that as the applied frequency approaches the natural frequency of internal resonators, i.e., 7 Hz the attenuation factor shows sharp increase and a maximum attenuation in displacement at this frequency. Thus, the proposed periodic foundation is theoretically capable of producing an ultra-low frequency bandgap that covers the major seismically active frequencies of the ground motion, hence being an effective solution for earthquake induced lateral loading especially due to S-waves for masonry, as well as stiff and flexible concrete or steel structure owing to the fact that the building sitting over the proposed periodic foundation will be subjected to filtered seismic wave due to the attenuation cause by the wave passage through periodic mass in mass structure.

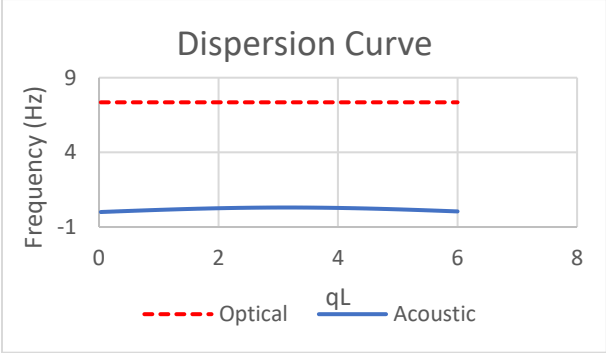

Figure 20. Dispersion Curve plotted between qL and Frequency for the proposed foundation.

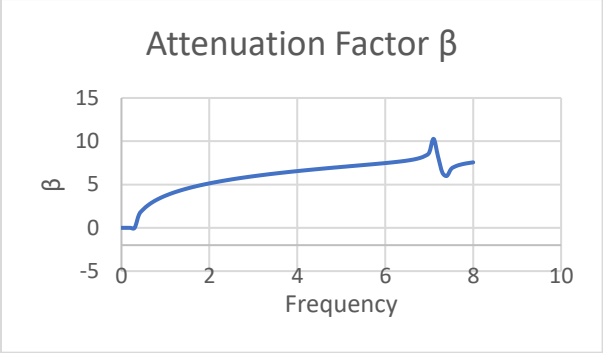

Figure 21. Graph between Frequency and Attenuation factor β for the proposed foundation.

4.2.1.2 Proposed Periodic Foundation (steel-wood arrangement)

Using $m_r = 2016\ kg\ , m_p = 30500\ kg, k_r = \ 4032000\frac{N}{m}\ and\ k_p = 30000\frac{N}{m}$ of the proposed periodic foundation, the following bandgap was obtained as illuminated in equation 12 and 13.

The frequency bandgap starts at:

$$f_{start} = \frac{1}{2\pi}\sqrt{\frac{\left[k_r(m_p + m_r) + 4k_p m_r\right] - \sqrt{\left[k_r(m_p + m_r) + 4k_p m_r\right]^2 - 16 m_r m_p k_p k_r}}{2 m_p m_r}}$$

$$= 0.30\ Hz \qquad (21)$$

The frequency bandgap ends at:

	$$f_{end} = \frac{1}{2\pi}\sqrt{\frac{[k_r(m_p + m_r)]}{m_p m_r}} = 1350\ Hz$$	22

Figure 22 shows the dispersion curves which indicates the frequency band gap from 0.30 Hz to 1350 Hz by the region between acoustical and optical branches. The bandgap is very wide and covers more than a thousand hertz in its range. Figure 23 shows that the attenuation factor β increases at a lower rate than steel-silicone resonator, yet still shows some attenuation when the properties of wood are integrated in the model. We do not visualize any peak in this graph, as opposed to the one for steel-silicone, as the resonant frequency is not encountered in the below 10 Hz range.

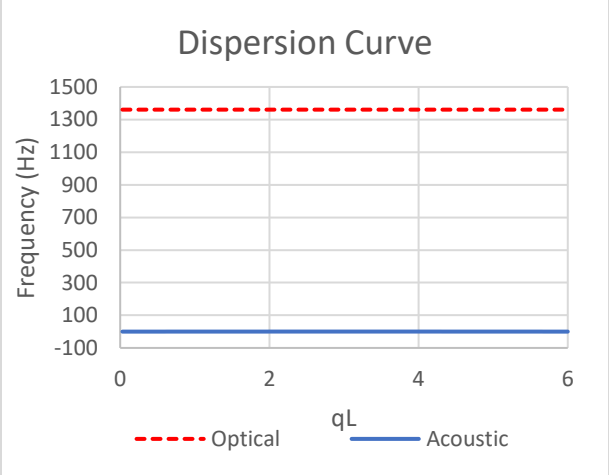

Figure 22. Dispersion Curve plotted between qL and Frequency for the proposed foundation.

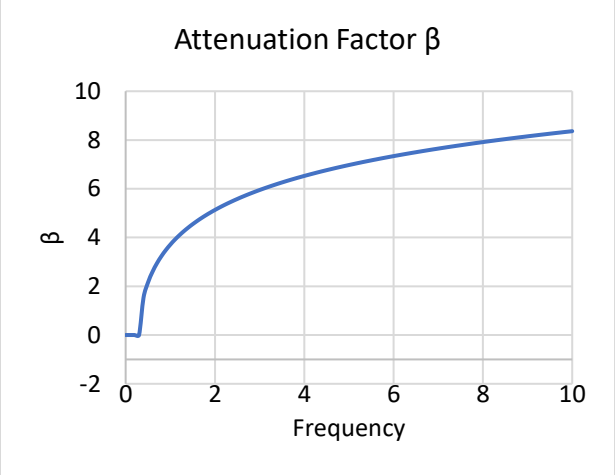

Figure 23. Graph between Frequency and Attenuation factor β for the proposed foundation.

Chapter Five

Conclusion

From the study of the proposed composite system that couples the properties of periodic foundation and the conventional base isolation system, it was found that a frequency bandgap is realized. Spatial decay of wave amplitude for waves with frequencies in the range of bandgap was clearly observed. The following conclusions are drawn:

1. The bandgap obtained from dispersion relation for scaled down prototype was achieved computationally and experimentally, hence validating the dispersion relation.
2. A higher attenuation was observed when the resonant frequency was within the concerned frequency band.
3. With increase in the number of panels, there is an increase in the overall attenuation within the bandgap. An average increase of 10% was observed when the number of panels was increased from one to 3.
4. Increase in load over the locally resonant panel increases the frictional forces, hence increasing the energy dissipation.
5. The scaled down prototype with 3 locally resonant periodic panels resulted in 73% maximum attenuation in displacement. The average attenuation in the frequency bandgap was observed to be 50%.
6. It was observed that the start of frequency bandgap is more sensitive to the stiffness of the silicone rubber pad providing horizontal connection between the overlaying panels.
7. The validation of dispersion relation and the theoretical results for the proposed periodic foundation panel shows that a very low and wide frequency bandgap covering principle frequencies of seismic waves is achievable. This bandgap also covers the resonant frequencies of common structures as well as important structures such as nuclear power plants.

The proposed periodic foundation is an effective wave of seismic isolation that overcomes the major drawbacks of conventional as well as modern seismic vibration mitigation devices. Such system can be employed without a major risk of amplification of seismic waves with frequencies less than the starting frequency of the bandgap as it covers the major portion of seismic waves frequency content. Such system can be improved easily with using local resonators with much lesser frequencies, which is easily achievable by increasing the mass of the resonator for which space is available, also the size of the cavity carrying the resonator can be easily increased.

References

1. Casablanca O, Ventura G, Garescì F, et al. Seismic isolation of buildings using composite foundations based on metamaterials. *Journal of Applied Physics*. 2018;123(17):174903. doi:10.1063/1.5018005

2. Zhao C, Zeng C, Huang H, et al. Preliminary study on the periodic base isolation effectiveness and experimental validation. *Engineering Structures*. 2021;226:111364. doi:10.1016/j.engstruct.2020.111364

3. Huang YN, Whittaker AS, Luco N. Seismic performance assessment of base-isolated safety-related nuclear structures. *Earthquake Engineering & Structural Dynamics*. 2010;39(13):1421-1442. doi:10.1002/eqe.1038

4. Naeim F, Kelly JM. *Design of Seismic Isolated Structures: From Theory to Practice*. John Wiley & Sons; 1999.

5. Xu YL, He Q, Ko JM. Dynamic response of damper-connected adjacent buildings under earthquake excitation. *Engineering Structures*. 1999;21(2):135-148. doi:10.1016/S0141-0296(97)00154-5

6. de Domenico D, Ricciardi G, Takewaki I. Design strategies of viscous dampers for seismic protection of building structures: A review. *Soil Dynamics and Earthquake Engineering*. 2019;118:144-165. doi:10.1016/j.soildyn.2018.12.024

7. Nagase T, Hisatoku T. Tuned-pendulum mass damper installed in crystal tower. *The Structural Design of Tall Buildings*. 1992;1(1):35-56. doi:10.1002/tal.4320010105

8. Losanno D, Spizzuoco M, Calabrese A. Bidirectional shaking-table tests of unbonded recycled-rubber fiber-reinforced bearings (RR-FRBs). *Structural Control and Health Monitoring*. 2019;26(9). doi:10.1002/stc.2386

9. Losanno D, Madera Sierra IE, Spizzuoco M, Marulanda J, Thomson P. Experimental assessment and analytical modeling of novel fiber-reinforced isolators in unbounded configuration. *Composite Structures*. 2019;212:66-82. doi:10.1016/j.compstruct.2019.01.026

10. Li HN, Sun T, Lai Z, Nagarajaiah S. Effectiveness of Negative Stiffness System in the Benchmark Structural-Control Problem for Seismically Excited Highway Bridges. *Journal of Bridge Engineering*. 2018;23(3). doi:10.1061/(ASCE)BE.1943-5592.0001136

11. Dong G, Zhang Y, Luo Y, Xie S, Zhang X. Enhanced isolation performance of a high-static–low-dynamic stiffness isolator with geometric nonlinear damping. *Nonlinear Dynamics*. 2018;93(4):2339-2356. doi:10.1007/s11071-018-4328-5

12. Shan J, Shi Z, Hu F, Yu J, Shi W. Stochastic optimal design of novel nonlinear base isolation system for seismic-excited building structures. *Structural Control and Health Monitoring*. 2018;25(7):e2168. doi:10.1002/stc.2168

13. Zhou Y, Chen P, Mosqueda G. Analytical and Numerical Investigation of Quasi-Zero Stiffness Vertical Isolation System. *Journal of Engineering Mechanics*. 2019;145(6). doi:10.1061/(ASCE)EM.1943-7889.0001611

14. Antoniadis IA, Kanarachos SA, Gryllias K, Sapountzakis IE. KDamping: A stiffness based vibration absorption concept. *Journal of Vibration and Control*. 2018;24(3):588-606. doi:10.1177/1077546316646514

15. Sapountzakis EJ, Syrimi PG, Pantazis IA, Antoniadis IA. KDamper concept in seismic isolation of bridges with flexible piers. *Engineering Structures*. 2017;153:525-539. doi:10.1016/j.engstruct.2017.10.044

16. Zhao Z, Zhang R, Jiang Y, Pan C. Seismic response mitigation of structures with a friction pendulum inerter system. *Engineering Structures*. 2019;193:110-120. doi:10.1016/j.engstruct.2019.05.024

17. Luo H, Zhang R, Weng D. Mitigation of liquid sloshing in storage tanks by using a hybrid control method. *Soil Dynamics and Earthquake Engineering*. 2016;90:183-195. doi:10.1016/j.soildyn.2016.08.037

18. De Domenico D, Ricciardi G. An enhanced base isolation system equipped with optimal tuned mass damper inerter (TMDI). *Earthquake Engineering & Structural Dynamics*. 2018;47(5):1169-1192. doi:10.1002/eqe.3011

19. de Domenico D, Ricciardi G. Optimal design and seismic performance of tuned mass damper inerter (TMDI) for structures with nonlinear base isolation systems. *Earthquake Engineering & Structural Dynamics*. Published online August 5, 2018. doi:10.1002/eqe.3098

20. Kushwaha MS, Halevi P, Dobrzynski L, Djafari-Rouhani B. Acoustic band structure of periodic elastic composites. *Physical Review Letters*. 1993;71(13):2022-2025. doi:10.1103/PhysRevLett.71.2022

21. Sigalas MM, Economou EN. Elastic and acoustic wave band structure. *Journal of Sound and Vibration*. 1992;158(2):377-382. doi:10.1016/0022-460X(92)90059-7

22. Zhou X, Liu X, Hu G. Elastic metamaterials with local resonances: an overview. *Theoretical and Applied Mechanics Letters*. 2012;2(4):041001. doi:10.1063/2.1204101

23. Lucklum F, Vellekoop MJ. Bandgap engineering of three-dimensional phononic crystals in a simple cubic lattice. *Applied Physics Letters*. 2018;113(20):201902. doi:10.1063/1.5049663

24. Liu H, Zhang Q, Zhang K, Hu G, Duan H. Designing 3D Digital Metamaterial for Elastic Waves: From Elastic Wave Polarizer to Vibration Control. *Advanced Science*. 2019;6(16):1900401. doi:10.1002/advs.201900401

25. Chuang KC, Lv XF, Wang DF. A tunable elastic metamaterial beam with flat-curved shape memory alloy resonators. *Applied Physics Letters*. 2019;114(5):051903. doi:10.1063/1.5084548

26. Chen Y, Qian F, Scarpa F, Zuo L, Zhuang X. Harnessing multi-layered soil to design seismic metamaterials with ultralow frequency band gaps. *Materials & Design*. 2019;175:107813. doi:10.1016/j.matdes.2019.107813

27. Jafari H, Yazdi MH, Fakhrabadi MMS. Damping effects on wave-propagation characteristics of microtubule-based bio-nano-metamaterials. *International Journal of Mechanical Sciences*. 2020;184:105844. doi:10.1016/j.ijmecsci.2020.105844

28. Liu Z, Zhang X, Mao Y, et al. Locally Resonant Sonic Materials. *Science (1979)*. 2000;289(5485):1734-1736. doi:10.1126/science.289.5485.1734

29. Croënne C, Lee EJS, Hu H, Page JH. Band gaps in phononic crystals: Generation mechanisms and interaction effects. *AIP Advances*. 2011;1(4):041401. doi:10.1063/1.3675797

30. Jia Z, Chen Y, Yang H, Wang L. Designing Phononic Crystals with Wide and Robust Band Gaps. *Physical Review Applied*. 2018;9(4):044021. doi:10.1103/PhysRevApplied.9.044021

31. le Pevelen DD. Small Molecule X-Ray Crystallography, Theory and Workflow. In: *Encyclopedia of Spectroscopy and Spectrometry*. Elsevier; 2010:2559-2576. doi:10.1016/B978-0-12-374413-5.00359-6

32. Li FL, Wang YS, Zhang C. A BEM for band structure and elastic wave transmission analysis of 2D phononic crystals with different interface conditions. *International Journal of Mechanical Sciences*. 2018;144:110-117. doi:10.1016/j.ijmecsci.2018.05.042

33. Dong J, Chen W, Zeng Z, Qin QH, Xiao Y. Analysis of wave band gaps in mechanical metamaterial based on Nelder–Mead method. *Engineering Analysis with Boundary Elements*. 2019;103:109-115. doi:10.1016/j.enganabound.2019.03.011

34. Matlack KH, Bauhofer A, Krödel S, Palermo A, Daraio C. Composite 3D-printed metastructures for low-frequency and broadband vibration absorption. *Proceedings of the National Academy of Sciences*. 2016;113(30):8386-8390. doi:10.1073/pnas.1600171113

35. Nimmagadda C, Matlack KH. Thermally tunable band gaps in architected metamaterial structures. *Journal of Sound and Vibration*. 2019;439:29-42. doi:10.1016/j.jsv.2018.09.053

36. Li Y, Cao S, Shen Y, Meng Y. Phononic band-gaps of Hoberman spherical metamaterials in low frequencies. *Materials & Design*. 2019;181:107935. doi:10.1016/j.matdes.2019.107935

37. Nateghi A, Sangiuliano L, Claeys C, Deckers E, Pluymers B, Desmet W. Design and experimental validation of a metamaterial solution for improved noise and vibration behavior of pipes. *Journal of Sound and Vibration*. 2019;455:96-117. doi:10.1016/j.jsv.2019.05.009

38. Moscatelli M, Ardito R, Driemeier L, Comi C. Band-gap structure in two- and three-dimensional cellular locally resonant materials. *Journal of Sound and Vibration*. 2019;454:73-84. doi:10.1016/j.jsv.2019.04.027

39. Li Z, Hu H, Wang X. A new two-dimensional elastic metamaterial system with multiple local resonances. *International Journal of Mechanical Sciences*. 2018;149:273-284. doi:10.1016/j.ijmecsci.2018.09.053

40. Meng H, Chronopoulos D, Fabro AT, Maskery I, Chen Y. Optimal design of rainbow elastic metamaterials. *International Journal of Mechanical Sciences*. 2020;165:105185. doi:10.1016/j.ijmecsci.2019.105185

41. Krushynska AO, Miniaci M, Bosia F, Pugno NM. Coupling local resonance with Bragg band gaps in single-phase mechanical metamaterials. *Extreme Mech Lett*. 2017;12:30-36. doi:10.1016/j.eml.2016.10.004

42. Lee T, Iizuka H. Bragg scattering based acoustic topological transition controlled by local resonance. *Physical Review B*. 2019;99(6):064305. doi:10.1103/PhysRevB.99.064305

43. Yuan B, Chen Y, Jiang M, Tang S, He M, Tu M. the Interaction of Resonance And Bragg Scattering Effects for the Locally Resonant Phononic Crystal with Alternating Elastic and Fluid Matrices. *Archives of Acoustics*. 2017;42(4):725-733. doi:10.1515/aoa-2017-0075

44. Yuan B, Humphrey VF, Wen J, Wen X. On the coupling of resonance and Bragg scattering effects in three-dimensional locally resonant sonic materials. *Ultrasonics*. 2013;53(7):1332-1343. doi:10.1016/j.ultras.2013.03.019

45. Brûlé S, Javelaud EH, Enoch S, Guenneau S. Experiments on Seismic Metamaterials: Molding Surface Waves. *Physical Review Letters*. 2014;112(13):133901. doi:10.1103/PhysRevLett.112.133901

46. Colombi A, Roux P, Guenneau S, Gueguen P, Craster R v. Forests as a natural seismic metamaterial: Rayleigh wave bandgaps induced by local resonances. *Scientific Reports*. 2016;6(1):19238. doi:10.1038/srep19238

47. Miniaci M, Krushynska A, Bosia F, Pugno NM. Large scale mechanical metamaterials as seismic shields. *New Journal of Physics*. 2016;18(8):083041. doi:10.1088/1367-2630/18/8/083041

48. Shi Z, Cheng Z, Xiang H. *Periodic Structures: Theory and Applications to Seismic Isolation and Vibration Reduction*.; 2017.

49. Palermo A, Krödel S, Marzani A, Daraio C. Engineered metabarrier as shield from seismic surface waves. *Scientific Reports*. 2016;6(1):39356. doi:10.1038/srep39356

50. Dertimanis VK, Antoniadis IA, Chatzi EN. Feasibility Analysis on the Attenuation of Strong Ground Motions Using Finite Periodic Lattices of Mass-in-Mass Barriers. *Journal of Engineering Mechanics*. 2016;142(9). doi:10.1061/(ASCE)EM.1943-7889.0001120

51. Pu X, Shi Z, Xiang H. Feasibility of ambient vibration screening by periodic geofoam-filled trenches. *Soil Dynamics and Earthquake Engineering*. 2018;104:228-235. doi:10.1016/j.soildyn.2017.10.022

52. Huang J, Shi Z. Application of Periodic Theory to Rows of Piles for Horizontal Vibration Attenuation. *International Journal of Geomechanics*. 2013;13(2):132-142. doi:10.1061/(ASCE)GM.1943-5622.0000193

53. Huang J, Shi Z. Attenuation zones of periodic pile barriers and its application in vibration reduction for plane waves. *Journal of Sound and Vibration*. 2013;332(19):4423-4439. doi:10.1016/j.jsv.2013.03.028

54. Cheng ZB, Shi ZF. Composite periodic foundation and its application for seismic isolation. *Earthquake Engineering & Structural Dynamics*. 2018;47(4):925-944. doi:10.1002/eqe.2999

55. Jia G, Shi Z. A new seismic isolation system and its feasibility study. *Earthquake Engineering and Engineering Vibration*. 2010;9(1):75-82. doi:10.1007/s11803-010-8159-8

56. Cheng Z, Shi Z. Novel composite periodic structures with attenuation zones. *Engineering Structures*. 2013;56:1271-1282. doi:10.1016/j.engstruct.2013.07.003

57. Yan Y, Laskar A, Cheng Z, et al. Seismic isolation of two dimensional periodic foundations. *Journal of Applied Physics*. 2014;116(4):044908. doi:10.1063/1.4891837

58. Yan Y, Cheng Z, Menq F, Mo YL, Tang Y, Shi Z. Three dimensional periodic foundations for base seismic isolation. *Smart Materials and Structures*. 2015;24(7):075006. doi:10.1088/0964-1726/24/7/075006

59. la Salandra V, Wenzel M, Bursi OS, Carta G, Movchan AB. Conception of a 3D Metamaterial-Based Foundation for Static and Seismic Protection of Fuel Storage Tanks. *Frontiers in Materials*. 2017;4. doi:10.3389/fmats.2017.00030

60. Basone F, Wenzel M, Bursi OS, Fossetti M. Finite locally resonant Metafoundations for the seismic protection of fuel storage tanks. *Earthquake Engineering & Structural Dynamics*. 2019;48(2):232-252. doi:10.1002/eqe.3134

61. Sun F, Xiao L. Bandgap Characteristics and Seismic Applications of Inerter-in-Lattice Metamaterials. *Journal of Engineering Mechanics*. 2019;145(9). doi:10.1061/(ASCE)EM.1943-7889.0001642

62. Bao J, Shi Z, Xiang H. Dynamic Responses of a Structure with Periodic Foundations. *Journal of Engineering Mechanics*. 2012;138(7):761-769. doi:10.1061/(ASCE)EM.1943-7889.0000383

63. Xiang HJ, Shi ZF, Wang SJ, Mo YL. Periodic materials-based vibration attenuation in layered foundations: experimental validation. *Smart Materials and Structures*. 2012;21(11):112003. doi:10.1088/0964-1726/21/11/112003

64. Shi Z, Huang J. Feasibility of reducing three-dimensional wave energy by introducing periodic foundations. *Soil Dynamics and Earthquake Engineering*. 2013;50:204-212. doi:10.1016/j.soildyn.2013.03.009

65. Cheng Z, Yan Y, Menq FM, et al. 3D periodic foundation-based structural vibration isolation. In: ; 2013.

66. Witarto W, Wang SJ, Yang CY, et al. Seismic isolation of small modular reactors using metamaterials. *AIP Advances*. 2018;8(4):045307. doi:10.1063/1.5020161

67. Calvi PM, Calvi GM. Historical development of friction-based seismic isolation systems. *Soil Dynamics and Earthquake Engineering*. 2018;106:14-30. doi:10.1016/j.soildyn.2017.12.003

68. de Domenico D, Gandelli E, Quaglini V. Adaptive isolation system combining low-friction sliding pendulum bearings and SMA-based gap dampers. *Engineering Structures*. 2020;212:110536. doi:10.1016/j.engstruct.2020.110536

69. Lin YS, Chan RWK, Tagawa H. Earthquake early warning-enabled smart base isolation system. *Automation in Construction*. 2020;115:103203. doi:10.1016/j.autcon.2020.103203

70. de Domenico D, Gandelli E, Quaglini V. Effective base isolation combining low-friction curved surface sliders and hysteretic gap dampers. *Soil Dynamics and Earthquake Engineering*. 2020;130:105989. doi:10.1016/j.soildyn.2019.105989

71. Ministry of Construction of the People's Republic of China. *Code for Seismic Design of Buildings*. China Architecture & Building Press; 2001.

72. CEN. *Eurocode 8: Seismic Design of Buildings. Part:1 General Rules, Seismic Actions and Rules for Buildings*. Publications Office of the European Union; 2004.

73. Cardone D, Gesualdi G. Influence of residual displacements on the design displacement of spherical friction-based isolation systems. *Soil Dynamics and Earthquake Engineering*. 2017;100:492-503. doi:10.1016/j.soildyn.2017.07.001

74. Habieb AB, Valente M, Milani G. Effectiveness of different base isolation systems for seismic protection: Numerical insights into an existing masonry bell tower. *Soil Dynamics and Earthquake Engineering*. 2019;125:105752. doi:10.1016/j.soildyn.2019.105752

75. Cancellara D, de Angelis F. A base isolation system for structures subject to extreme seismic events characterized by anomalous values of intensity and frequency content. *Composite Structures*. 2016;157:285-302. doi:10.1016/j.compstruct.2016.09.002

76. Mazza F, Labernarda R. Effects of nonlinear modelling of the base-isolation system on the seismic analysis of r.c. buildings. *Procedia Structural Integrity*. 2018;11:226-233. doi:10.1016/j.prostr.2018.11.030

77. Mayes RL, Naeim F. Design of Structures with Seismic Isolation. In: *The Seismic Design Handbook*. Springer US; 2001:723-755. doi:10.1007/978-1-4615-1693-4_14

78. Heaton TH, Hall JF, Wald DJ, Halling MW. Response of High-Rise and Base-Isolated Buildings to a Hypothetical M_w 7.0 Blind Thrust Earthquake. *Science (1979)*. 1995;267(5195):206-211. doi:10.1126/science.267.5195.206

79. Bhandari M, Bharti SD, Shrimali MK, Datta TK. The Numerical Study of Base-Isolated Buildings Under Near-Field and Far-Field Earthquakes. *Journal of Earthquake Engineering*. 2018;22(6):989-1007. doi:10.1080/13632469.2016.1269698

80. Pinkaew T, Lukkunaprasit P, Chatupote P. Seismic effectiveness of tuned mass dampers for damage reduction of structures. *Engineering Structures*. 2003;25:39-46. doi:10.1016/S0141-0296(02)00115-3

81. Lee C, Goda K, Hong H. Effectiveness of using tuned-mass dampers in reducing seismic risk. *Structure and Infrastructure Engineering*. 2012;8:141-156. doi:10.1080/15732470903419669

82. N KDP, Abdelraheem FA. TMD effectiveness for steel high-rise building subjected to wind or earthquake including soil-structure interaction. *Wind and Structures*. 2020;30(4):423-432. doi:10.12989/WAS.2020.30.4.423

83. Boccamazzo A, Carboni B, Quaranta G, Lacarbonara W. Seismic effectiveness of hysteretic tuned mass dampers for inelastic structures. *Engineering Structures*. 2020;216:110591. doi:10.1016/j.engstruct.2020.110591

84. Woo SS, Lee SH, Chung L. Seismic response control of elastic and inelastic structures by using passive and semi-active tuned mass dampers. *Smart Structures and Systems*. 2011;8(3):239-252. doi:10.12989/sss.2011.8.3.239

85. Sgobba S, Marano GC. Optimum design of linear tuned mass dampers for structures with nonlinear behaviour. *Mechanical Systems and Signal Processing*. 2010;24(6):1739-1755. doi:10.1016/j.ymssp.2010.01.009

86. Duque EP, Inaudi JA, García VJ. EFICIENCIA DE AMORTIGUADORES DE MASA SINTONIZADA EN ESTRUCTURAS CON COMPORTAMIENTO ELASTO-PLÁSTICO SOMETIDAS A CARGAS SÍSMICAS EFFICIENCY OF TUNED MASS DAMPER ATTACHED TO STRUCTURES WITH ELASTOPLASTIC BEHAVIOR AND SUBJECTED TO SEISMIC EXCITATION. *Accidentes e Infraestructura Civil*. 2007;15(1):59.

87. García VJ, Duque EP, Inaudi JA, Márquez CO, Mera JD, Rios AC. Pendulum tuned mass damper: optimization and performance assessment in structures with elastoplastic behavior. *Heliyon*. 2021;7(6):e07221. doi:10.1016/j.heliyon.2021.e07221

88. Anajafi H, Poursadr K, Roohi M, Santini-Bell E. Effectiveness of Seismic Isolation for Long-Period Structures Subject to Far-Field and Near-Field Excitations. *Frontiers in Built Environment*. 2020;6. doi:10.3389/fbuil.2020.00024

89. Phani AS, Woodhouse J, Fleck NA. Wave propagation in two-dimensional periodic lattices. *J Acoust Soc Am*. 2006;119(4):1995-2005. doi:10.1121/1.2179748

90. Shi Z, Cheng Z, Xiang H. Seismic isolation foundations with effective attenuation zones. *Soil Dynamics and Earthquake Engineering*. 2014;57:143-151. doi:10.1016/j.soildyn.2013.11.009

91. Cheng ZB, Shi ZF. Composite periodic foundation and its application for seismic isolation. *Earthquake Engineering & Structural Dynamics*. 2018;47(4):925-944. doi:10.1002/eqe.2999

92. Simitses GJ, Rezaeepazhand J. Structural similitude for laminated structures. *Composites Engineering*. 1993;3(7-8):751-765. doi:10.1016/0961-9526(93)90094-Z

93. Eydani Asl M, Niezrecki C, Sherwood J, Avitabile P. Vibration prediction of thin-walled composite I-beams using scaled models. *Thin-Walled Structures*. 2017;113:151-161. doi:10.1016/j.tws.2017.01.020

94. Sun F, Xiao L, Bursi OS. Optimal design and novel configuration of a locally resonant periodic foundation (LRPF) for seismic protection of fuel storage tanks. *Engineering Structures*. 2019;189:147-156. doi:10.1016/j.engstruct.2019.03.072

95. Zhao C, Zeng C, Huang H, et al. Preliminary study on the periodic base isolation effectiveness and experimental validation. *Engineering Structures*. 2021;226:111364. doi:10.1016/j.engstruct.2020.111364